Design and Analysis of Mirror Modules for IXO and Beyond

Ryan S. McClelland*[a], Cory Powell[b], Timo T. Saha[b], William W. Zhang[b]
[a]SGT Inc. 7701 Greenbelt Road, Suite 400, Greenbelt, Maryland 20770, USA
[b]NASA Goddard Space Flight Center (GSFC), Greenbelt, MD USA 20771, USA

ABSTRACT

Advancements in X-ray astronomy demand thin, light, and closely packed thin optics which lend themselves to segmentation of the annular mirrors and, in turn, a modular approach to the mirror design. The functionality requirements of such a mirror module are well understood. A baseline modular concept for the proposed International X-Ray Observatory (IXO) Flight Mirror Assembly (FMA) consisting of 14,000 glass mirror segments divided into 60 modules was developed and extensively analyzed. Through this development, our understanding of module loads, mirror stress, thermal performance, and gravity distortion have greatly progressed. The latest progress in each of these areas is discussed herein. Gravity distortion during horizontal X-ray testing and on-orbit thermal performance have proved especially difficult design challenges. In light of these challenges, fundamental trades in modular X-ray mirror design have been performed. Future directions in module X-ray mirror design are explored including the development of a 1.8 m diameter FMA utilizing smaller mirror modules. The effect of module size on mirror stress, module self-weight distortion, thermal control, and range of segment sizes required is explored with advantages demonstrated from smaller module size in most cases.

Keywords: International X-Ray Observatory, IXO, Module, Flight Mirror Assembly, FMA, X-Ray Optics

1. INTRODUCTION

Larger effective area and higher resolution optics are required to enable future discoveries by X-ray observatories [1]. The effective area of a space based X-ray mirror is limited by the filling factor allowed for by the mirror technology, the launch mass capability, the fairing diameter, and mirror cost. The use of densely packed thin foil mirrors has been adopted to increase the filling factor while reduce the mirror mass, diameter, and cost. As the diameter a thin foil mirrors increase, it becomes increasingly difficult and expensive to make full annular mirrors. The largest full annulus thin foil mirror flown was on the XMM-Newton mission, having a 350 mm radius, 0.75 mm thickness, and ~15 arc-sec Half Power Diameter (HPD) resolution [2].

To fabricate thin foil mirrors with larger radii, lighter weight, and/or greater resolution a segmented approach, dividing the annulus into several partial mirrors, has been adopted. The segmented mirror approach lends itself to modularization with the mirror consisting of many independently integrated modules, with each wedge-shaped module containing many radially nested mirror segments, which are subsequently co-aligned (Figure 1). This approach has been used successfully on flown missions including BBXRT and Astro-E [3]. Aside from the convenience of segmenting the annular mirrors, the modular approach has several other important benefits. Modules can be independently integrated and verified allowing for parallel processing as well as creation of verified spares should a flight module be damaged. The process of repeating integration of many identical modules allows for potential industrialization and automation in order to increase manufacturing speed and lower cost. Cost can also be saved with the modular approach by re-using the polished area of the forming mandrel to create multiple segments. For the full annular mirror, the polished area required to create each mirror is, at a minimum, equal to the mirror area. For the segmented approach, the polished area required decreases as the number of segments increases.

This paper describes the extensive module design, analysis, and environmental testing performed in the development of the proposed IXO mission. Detailed analysis usually reserved for mature flight projects, such as Couple Loads Analysis (CLA), Structural Thermal Optical Performance (STOP) analysis, and coupled structure and mirror stress analysis have been performed on the IXO module design and will be useful to inform future modular mirror designs.

*ryan.s.mcclelland@nasa.gov; phone 1 301 286-8615

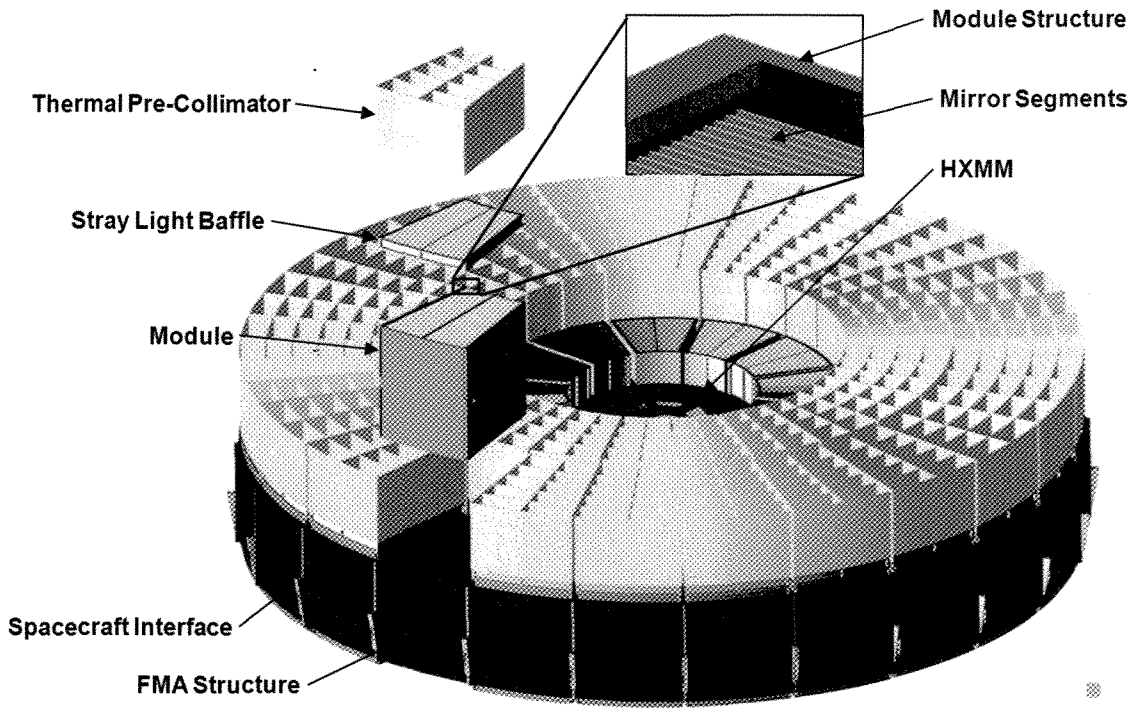

Figure 1. Exploded view of the proposed IXO FMA illustrating the modular approach. Each wedged shaped module contains many radially nested segments.

1.1 Functionality of the Mirror Module

In order to design an appropriate mirror module, the functionality of the module must be well defined and understood. Fundamentally, the module stably holds many mirror segments in alignment relative to one another. This is particularly important for designs where the primary and secondary mirrors are separate segments aligned within the same module due to the high sensitive of angular resolution to primary-secondary mirror misalignment. In addition to the alignment, the figure of the segments within the module also must be stable throughout the module life cycle.

The module design must allow for integration of the mirror segments and not distort as additional segments are added, requiring a high structural stiffness. Testability of the module also requires high structural stiffness as the self weight distortion of the module can cause large differences between the as-tested performance and on-orbit performance, especially when the module is tested with the optical axis horizontal.

Alignment and figure stability must be maintained after transportation and launch environments, requiring linear elastic structural behavior. On-orbit, the module must maintain stability for the duration of the mission while subject to vacuum and the mission thermal environment. The module may also provide on-orbit thermal control to maintain the required spatial and temporal temperature stability of both the mirrors and module structure (Figure 2).

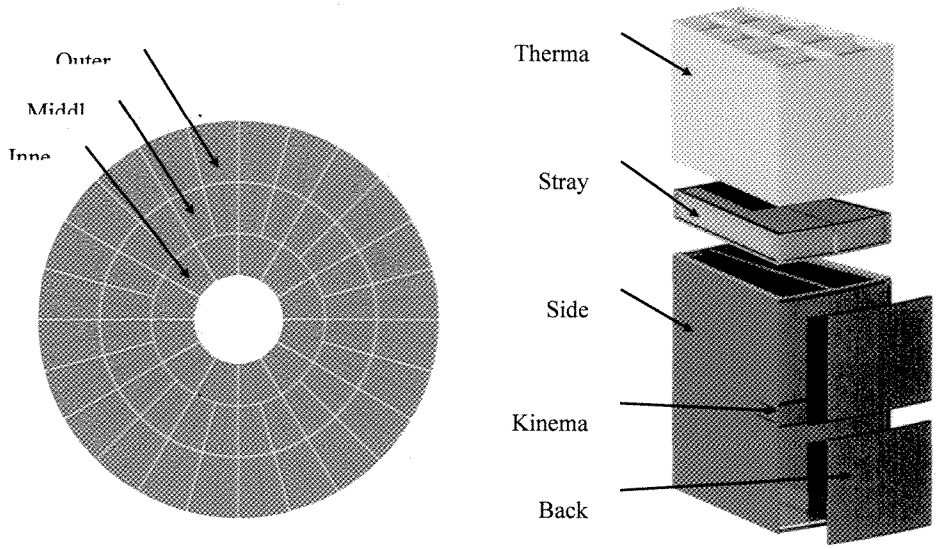

Figure 2. Top view of FMA with primary structure hidden illustrating the12/24/24 module layout (left) and exploded view of a middle ring module (right).

1.2 Slumped Glass Mirror Technology Overview

The mirror technology assumed for the module designs presented in this paper, currently in development at NASA GSFC, consists for 0.4 mm thick glass sheets slumped over polished convex mandrels [4]. The mirror segments thus formed are cut to size (200 mm axial length and variable azimuthal span), coated with a thin layer of iridium, and temporarily mounted to a structure allowing for rigid body manipulation. Pairs of mirrors are then aligned to a common focus using rigid body manipulation, permanently bonded into the module structure, then released from the temporary mount. Once the module is fully populated with mirror segments, the back of the module is closed out with a protective panel and the assembly is tested, as shown in Figure 2 (right).

1.3 IXO Flight Mirror Assembly (FMA) Overview

The proposed 3.2 m IXO FMA consists of 60 Soft X-ray Telescope (SXT) modules, each containing approximately 200-300 mirror segments, mounted into the FMA primary structure as shown in Figure 1. The inner ring has 12 modules and the middle and outer rings have 24 modules each. Table 1 gives a breakdown of the size, mass, and effective area of the three types of modules. Each module has additional thermal and optical elements mounted to it, including a thermal pre-collimator and a Stray Light Baffle (SLB) or thermal shield as shown in Figure 2. The Hard X-ray Mirror Module (HXMM) is mounted into a central hole in the primary structure. Note that the term 'module' in this paper generally refers to the SXT modules rather than the HXMM. The total effective area of this FMA design is 3.2 m^2 at 1.25 keV and 0.82 m^2 at 6 keV, the target resolution is 5 acr-sec HPD, and the mass is 1750 kg.

Table 1. Parameters of the inner, middle and outer modules including effective area of individual modules.

Ring	Inner	Middle	Outer
Modules per Ring	12	24	24
Nominal Azimuthal Span (degrees)	30	15	15
Number of Segments in Module	286	230	206
Azimuthal Span of Smallest Mirror (mm)	167	166	275
Azimuthal Span of Largest Mirror (mm)	335	263	392
Module Mass (kg)	22.6	15.7	21.9

Effective Area per module at 1.25 keV (m^2)	0.038	0.040	0.074
Effective Area per module at 6.0 keV (m^2)	0.031	0.018	0.001

2. PROGRESS ON IXO MODULE DESIGN AND ANALYSIS

2.1 Module Structure Material Selection

Trade studies have been performed to select the best material for the mirror module structure. The driving goals are to minimize mass, structural obscuration, mechanical deformation, and thermal distortion. To minimize the mass and mechanical deformation, a material with a high stiffness to weight ratio (specific stiffness) is desired. Less obviously, to minimize structural obscuration, a material with a high absolute stiffness (Young's modulus) is desired. Since any volume of structure necessarily detracts from the module effective area, maximizing the stiffness within a fixed volume is desired, perhaps even at the cost of increased mass.

To minimize thermal distortion caused by bulk temperature change, a material with a CTE matching D263 glass is desired. Unfortunately, common aerospace structural metals such as aluminum, stainless steel, and titanium have a CTE well above the 6.28 parts per million (ppm) per °C while common aerospace composite materials such as M55J/954-3 Carbon Fiber Reinforced Plastic (CFRP) have a CTE well below 6.28 ppm/°C. Metal Matrix Composites (MMCs) can provide nearly matching CTE, light weight, and excellent stiffness, but are very difficult and expensive to work with. Table 2 lists materials under consideration for the module structure along with a few reference materials.

Table 2. Mechanical and thermal properties for potential module structure materials and reference materials. The CTE Mismatch Error is predicted based on the STOP sensitivity study and the expected bulk temperature change of 0.5°C through integration, testing, and on-orbit operation.

Material	Density (kg/m^3)	Young's Modulus (GPa)	Specific Stiffness ($10^6 m^2/s^2$)	CTE (ppm/°C)	CTE Mismatch Error (arc-sec HPD)	Comments
M55J/954-3 CFRP	1688	104	62	-0.23	9.8	Poor CTE match, complex fabrication
AF45 Glass	2720	66	24	4.18	3.2	Alternate mirror segment glass
Alloy 42 (Fe Ni Alloy)	8110	145	18	4.48	2.7	Metal designed to match AF45 glass
TiSiC MMC	3930	200	51	5.90	0.6	Good properties, difficult to fabricate
D263 Glass	2510	73	29	6.28	0.0	Baseline mirror segment glass
T300/E-Glass composite	1700	32	19	6.28	0.0	Perfect CTE match, low stiffness
Custom Fe Ni Alloy	8359	138	17	6.28	0.0	Perfect CTE match, machinable, heavy
E-60 Beryllium MMC	2531	331	131	6.50	0.3	Excellent properties, difficult to fabricate
Kovar F15 (Fe Ni alloy)	8359	138	17	6.67	0.6	Good CTE match, machinable, heavy
Ti6Al4V Titanium	4430	114	26	8.88	3.9	Moderate CTE match, machinable
410 Series Stainless Steel	7800	200	26	9.90	5.4	Moderate CTE match, machinable
Beryllium S-200FH	1850	303	164	11.4	7.7	Poor CTE match, special machining
Aluminum 6061-T6	2700	69	26	22.6	24.5	Poor CTE match, low cost, machinable

It can be seen from Table 2 that two iron/nickel metal alloys, one CFRP, and two MMCs have well matched CTEs, expected to cause less than 1.0 arc-sec HPD error. Each has significant disadvantages. The iron/nickel metal alloys have good CTE matching, good machinability, but poor specific stiffness. The custom T300/E-Glass composite layup, developed and tested by NASA GSFC for the IXO mission, consists of both carbon and glass fibers that can be tuned by adjusting the resin volume to have a perfect in-plane CTE match with D263 glass. However, the absolute stiffness is very poor and potential distortions caused by the Coefficient of Moisture Expansion (CME) and high out-of-plane CTE need to be mitigated by extensive analysis and testing. The MMCs, especially Brush Wellman E-60, offer excellent properties including well matched CTE and high specific and absolute stiffnesses; however, they cannot be machined easily.

Based on this material trade study, Kovar F15 has been chosen as the baseline material for the module structure. Due to its reasonable cost and good machinablity, Kovar F15 is already extensively used in slumped glass mirror technology development. The custom CTE matched iron/nickel alloy would be preferred if it can be economically produced. If future mass savings are required, a MMC material may be desirable despite the increased cost and complexity of module fabrication. The custom T300/E-Glass composite is an unlikely candidate material due to the low absolute stiffness causing large structural obscuration as well as CME and out-of-plane CTE concerns.

2.2 Coupled Loads Analysis (CLA)

In order to determine the stresses the module and glass mirror segments must endure during launch, the acceleration loads they will experience must be quantified. These accelerations are used as quasi-static design loads in stress analysis. Typically, for a space flight project, loads derived from generic mass-acceleration curves are used in the preliminary design phase and loads derived from Coupled Loads Analysis, which involve the simulation of the entire launch vehicle by the launch vehicle provider, are used in the detailed design phase. In the case of IXO, an intermediate fidelity Sine Response Analysis (SRA) was performed which takes the stiffness of the observatory into account without having to involve the launch vehicle provider [5]. More recently, a full CLA was run for IXO by the Kennedy Space Center (KSC) assuming the Atlas 551 launch vehicle. The decrease in quasi-static design loads as the load determination fidelity increases can be seen in Table 3.

Table 3. Evolution of the enveloping quasi-static design loads used in IXO module design and analysis. Coupled Loads Analysis provides the lowest and most realistic loads.

Load Determination Method	Generic Mass-acceleration Curve	Sine Response Analysis	Coupled Loads Analysis
Axial Load (g)	22.0	18.0	9.2
Lateral Load (g)	22.0	8.5	2.5

To obtain worst case CLA loads, the mass of the observatory Finite Element Model (FEM) was scaled up to the maximum launch vehicle lift capability including 208 kg added to the FMA. Maximum interface forces were recovered for the FMA, modules, and other observatory sub-assemblies for the seven launch events: (1) liftoff, (2) transonic, (3) maximum dynamic pressure (MaxQ), (4) Solid Rocket Booster (SRB) jettison, (5) maximum axial acceleration, (6) booster engine cutoff, (7) centaur cutoff. The maximum interface force vector components are then divided by the sub-assembly mass to obtain the maximum acceleration loads for each sub-assembly. Due to the dynamics of the FMA primary structure the inner module experiences the highest acceleration as expected. Maximum accelerations of 6.14 g axial and 1.69 g lateral occur during the maximum axial acceleration and transonic events respectively. A Modeling Uncertainly Factor (MUF) of 1.5 is applied to the accelerations in order to account for the relative immaturity of the FEM, yielding the quasi-static loads shown in Table 2. The reduction in quasi-static loads by a factor of 2-3 between the SRA and CLA yields a corresponding decrease in predicted module and mirror segment stresses allowing for greater margins, mass savings, and/or decreased structural obscuration through design refinement.

These results are applicable to other X-ray mirror assemblies with the following assumptions: (1) the FMA is similarly mounted near the launch vehicle separation plane, (2) the natural frequencies of the FMA are the same or higher, (3) the launch vehicle is similar, (4) the loads are scaled by ratio of the FMA masses, (5) the MUF is increased.

2.3 Mirror Stress Analysis

Previously, the quasi-static design loads from the SRA were applied directly to a detailed FEM of the mirror segments in order to obtain mirror stresses [5]. Since the module is relatively stiff (first mode 70 Hz) it was assumed the influence of the module distortion on the mirror stress was relatively low. Stress was low compared to the statistically determined mirror allowable of 40 MPa resulting in high Margins of Safety (MS).

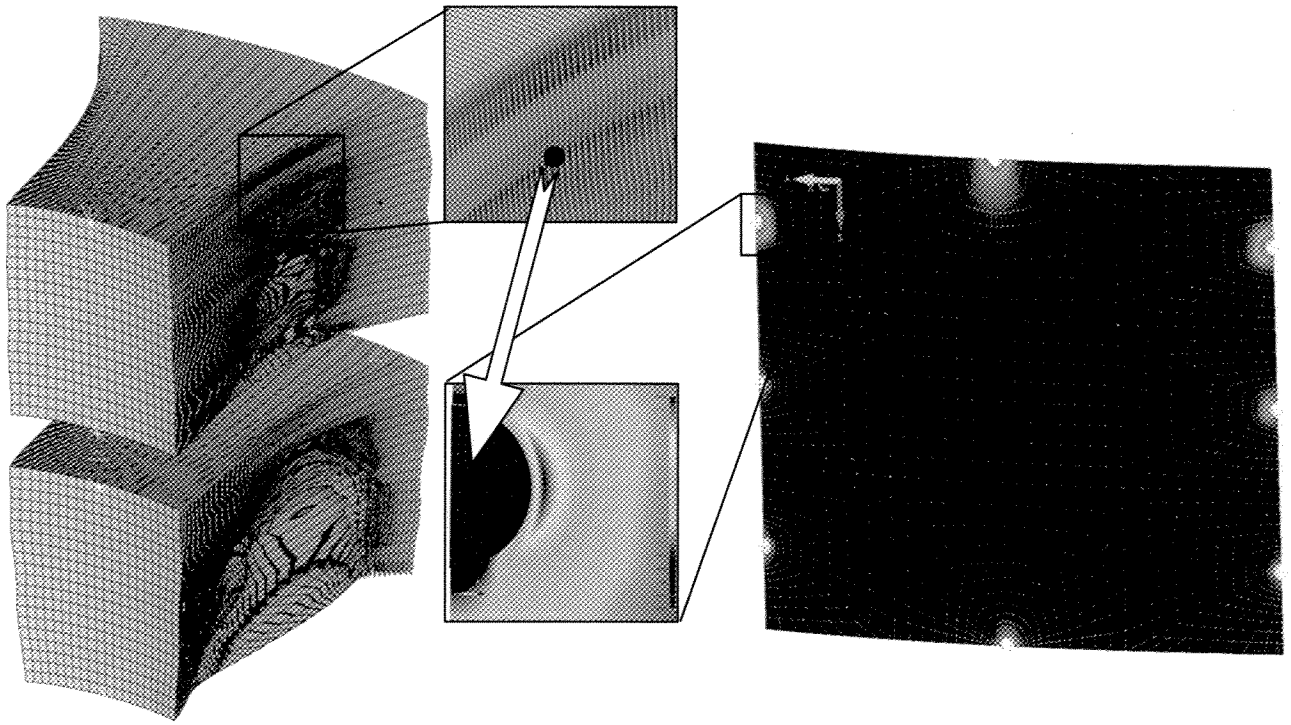

Figure 3. Displacements and rotations from mirror bond constraint locations of the overall module FEM (left) are mapped onto the detailed mirror segment FEM (right) for stress analysis. The maximum stress occurs directly adjacent to the bond pints. Combined 9.2 g axial, 2.5 g radial load case shown.

Recently, the assumption of low influence due to the flexibility of the module structure was checked and found to be erroneous. Due to the 206 mirror segments represented in the outer module FEM, detailed modeling of each segment is not computationally feasible. Instead, relatively coarse 21x21 node FEMs are used to represent the stiffness of the mirrors within the module FEM then displacements and rotations at the mirror bonding points are recovered and applied to a 30,000 node FEM of the most highly stressed mirror segments to replicate the stress state (Figure 3). As shown in Table 4, with the inclusion of the module deformations the stress is greater than an order of magnitude higher than the previously determine stress, though Margins of Safety are still positive in both cases.

Table 4. Maximum Principal Stress in 1045P mirror segment for 9.2 g vertical 2.5 g lateral quasi-static load case. Stress is much higher when module distortions are factored in. Margins of Safety are calculated versus a 40 MPa allowable stress.

Case	Case Description	Max Principal Stress (MPa)	Margin of Safety
1	Quasi-static loads directly applied to mirror FEM	0.84	14.9
2	Module distortions applied to mirror FEM	10.58	0.26
3	Case 2 with Young's Modulus of module structure doubled	8.44	0.58

To examine the sensitivity of the mirror stress to the module stiffness, the Young's Modulus of the module structure was doubled from 138 GPa (Kovar F15 material assumed) to 276 GPa. The stress was reduced by 20%. To further explore the relationship of the module deflection to the module structural design, the side walls of the module can be approximated as simply supported beams with the acceleration loads applied to the module and mirrors approximated as a uniformly distributed load. In this case the maximum defection would be:

$$\delta = -\frac{5wL^4}{384EI} \tag{1}$$

Where δ is the deflection, w is the load per unit length, L is the length of the beam, E is the Young's Modulus, and I is the moment of inertia of the beam cross section. It can be seen in equation (1) that the deflection is the most sensitive to the length of the beam (which represents the module side wall). Based on this approximation, reducing the module size in the radial direction would significantly decrease the mirror stress though a corresponding increase in the number of modules is required. For example, reducing the module radial size by half would be expected to reduce the maximum deflection by a factor of 16, though twice as many modules would be needed to house the mirror segments. Further trade studies investigating the optimum module size are addressed in sections 2.5 and 3.2 below.

2.4 Structural Thermal Optical Performance (STOP) Analysis

Previously, STOP sensitivity analysis was performed on the module FEM in order to determine which thermal gradients were the most damaging to the optical performance [5]. Gradients between the module structure and mirror segments were shown to cause the most distortion, with a sensitivity of 20 arc-sec HPD per degree C. Recently, full STOP analysis was performed, including an observatory thermal model, application of worst case on-orbit thermal loading, mapping of temperatures from the module thermal model to a matching FEM model, determination of the resulting thermal distortion, and ray tracing of the resulting optical performance (Figure 4). The outer module was shown to have the worst case thermal gradients due to its proximity to the spacecraft boundary.

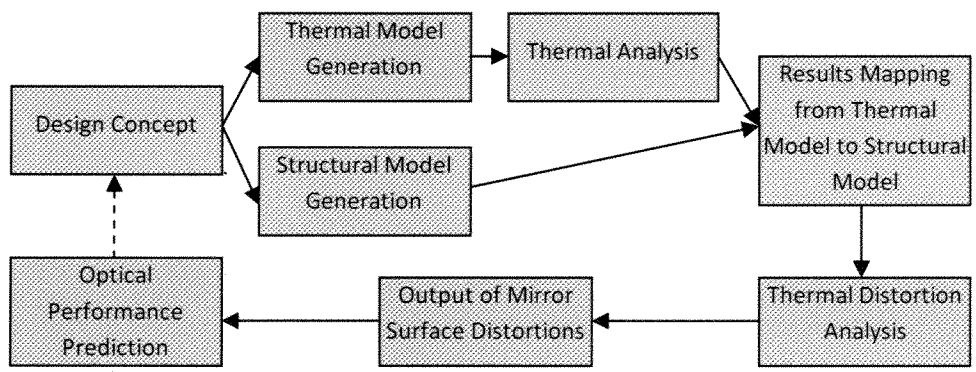

Figure 4. STOP analysis process flow. Once the optical performance prediction is complete iteration takes place as needed.

The thermal control system modeled includes a thermal pre-collimator with heated and passive portions, heated module walls, and a heated section of the telescope metering structure nearest the FMA [6]. The objective of the thermal control system is to replace the heat lost from the modules, which operate at room temperature, to cold space and maintain temperature uniformity across the module structure and mirror segments.

Generating the hundreds of unique mirror segment FEMs within the module with sufficient accuracy and element density to allow for ray-traced optical performance prediction is particularly challenging. Custom software was written to allow the segment FEMs to be automatically generated with the desired mesh density based on the optical prescription file. Additional custom software was written to extract the FEA output and ray-trace the results to generate performance predictions for both individual segments and entire modules. Performance predictions are based on the low order surface deformations and equations published in reference [7].

Table 5. STOP analysis results showing effects of modification to the thermal design. Case 1 models the initial thermal control design including mirror segments coated with iridium on the reflecting side only.

Case	Case Description	Module HPD (arc-sec)	Module RMSD (arc-sec)
1	Nominal case	33.8	45.2
2	Case 1 with perfect structure to mirror CTE match	32.3	44.0
3	Case 1 with no module wall heaters, walls coated black	37.4	62.6
4	Case 1 with mirror kinematically mounted	22.2	36.7
5	Case 1 with gold coating on back of mirror segments	8.1	14.1
6	Case 5 with mirror additional pre-collimator vanes	9.1	20.6
7	Case 5 with mirror kinematicaly mounted	6.6	10.2
8	Case 5 with improved heater set-points	6.5	12.3
9	Case 5 with pre and post collimators	11.6	21.8
10	Case 5 with mirror conductivity set to silicon	6.0	11.7

The most recent STOP analysis results are presented in Table 5. The thermal and mechanical designs have gone through many iterations attempting to improve the predicted module performance. Case 1 was the first attempt at performing the full STOP analysis on the module and the results were very poor relative to the IXO requirement allocation of 1.0 arc-sec HPD for thermal distortion, even though the maximum thermal gradient over the module in this case was only ±0.6°C. In order to determine the source of the distortion, several other cases were tried. It can be seen by the small difference between Case 1 and Case 2 results that the CTE mismatch between the D263 glass and Kovar F15 structure has a minimal effect. Eliminating the wall heaters in order to reduce the gradient between the mirrors and module structure results in worse performance as seem in Case 3. The results improve in Case 4 by 34% when a kinematic mirror mount is artificially assumed which indicates a significant portion of the error is generated by distortion of the module structure. However, the majority of the distortion still comes from the thermal gradients on the mirrors themselves as indicated by the large remaining error when the mirrors are allowed to expand or contract freely.

The largest improvement derives from coating the back of the mirror with a low emittance coating (vapor deposited gold in this case) in addition to the front (nominally coated with iridium) in order to minimize radiation of heat to space(Case 5). Improvements beyond the Case 5 are marginal. Adding additional thermal pre-collimator vanes, and adding post-collimators in addition to pre-collimators doe not improve the results (Cases 6 and 9). Assuming kinematic mounting improves the results relative to Case 5 by 18%, though a similar improvement is also realized by modifying the heater set points (Cases 7 and 8). Finally, an incremental improvement is realized by artificially increasing the conductivity of the mirror segments to that of silicon (Case 10).

The majority of the thermal distortion is being caused by axial gradients over the mirror segments as shown in Figure 5. This gradient results in a relatively constant ~6 arc-sec error throughout the module with the exception of the first couple dozen segments. Additional heater set point adjustment is expected to smooth the error over the entire module

eliminating any effect due to module radial size.

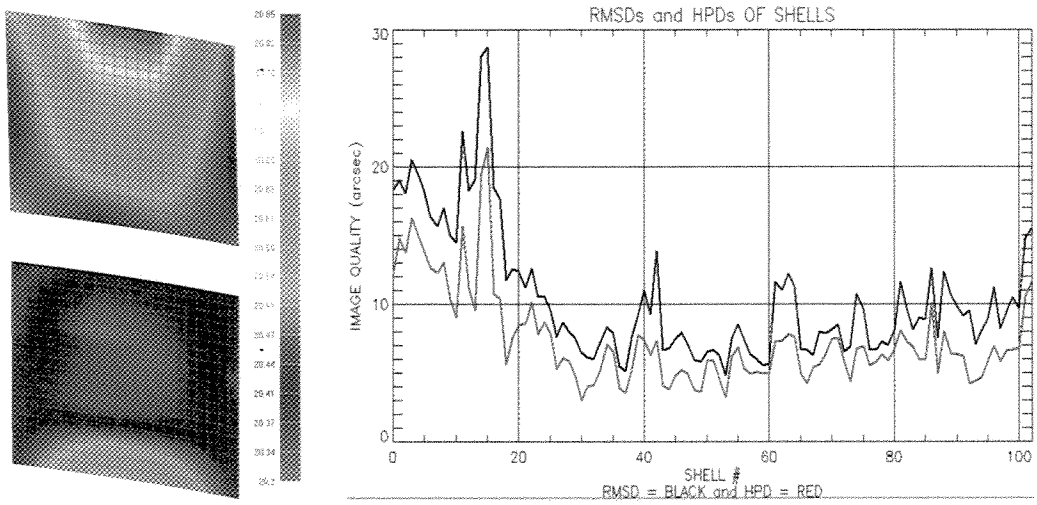

Figure 5. Temperature gradient of 0.5°C over a mirror pair based on Case 8 (right). The resulting HPD and RMSD error are relatively constant across all the segments in the module with the exception of the innermost ~25 segments.

The best results currently obtained are approaching the level that would be acceptable for a 10" arc-sec HPD X-ray mirror; however, significant improvements would need to be made to achieve a 5 arc-sec HPD telescope. Trade studies to improve the thermal and mechanical design are on-going.

2.5 Gravity Distortion During Integration and Test (I&T)

The module must be sufficiently stiff to prevent unacceptable deformation during mirror integration and X-ray testing. During integration, the module is kinematically supported with its optical axis vertical. This vertical orientation serves to minimize the distortion of the module walls and mirrors segments due to gravity. As shown in Table 6, Case 1 the self-weight distortion of mirrors held in this orientation is negligible if the finite stiffness of the module is ignored. Once the effect of the module distortion is considered the HPD error increases by an order of magnitude as shown in Case 2, though it is still within the IXO requirement for gravity release error. Since the module is populated under gravity the mirrors will be installed with the module already distorted. When that distortion is relieved under micro-gravity conditions, the error will be at most 1.2 arc-sec HPD or less since the module will be less distorted when the first segments are installed due to less mirror mass pulling on the module.

Table 6. Performance prediction of modules subject to gravity loads.

Case	Case Description	Module HPD (arc-sec)	Module RMSD (arc-sec)
1	Module vertical (1 g in z axis), module infinitely stiff	0.1	0.4
2	Module vertical (1 g in z axis)	1.2	1.8
3	Module horizontal (1 g in x axis), module infinitely stiff	2.5	19.1
4	Module horizontal (1 g in x axis)	40.8	104.0

Due to the long evacuated tube required for full aperture X-ray testing the ability to test with the optical axis horizontal is strongly desired. All current large aperture X-ray beamline facilities require horizontal testing. In this orientation, the edges of the thin mirror segments deflect under gravity creating sag errors which add constructively between the primary and secondary (Case 3). The localization of this effect to the mirror edges is evidenced by the large RMSD. As shown in Case 4, once the finite stiffness of the module is considered, the error becomes unacceptably high. This effect, which renders the module untestable in the horizontal orientation, can be mitigated by (1) supporting the module with a stiffening structure during testing (2) reducing the module radial size as described in section 2.3 or (3) testing the module

in a vertical orientation. Vertical testing could be accomplished testing in Extreme Ultraviolet (EUV) wavelengths [8], a vertical scanning X-ray beam, or a large aperture vertical X-ray beamline facility. Further development is required in this area.

3. FUTURE DIRECTIONS IN MODULE AND FMA DESIGN

3.1 Design of a 1.8 meter diameter FMA

Near future X-ray astrophysics missions are likely to be less ambitious than IXO in terms of effective area and perhaps angular resolution. As a primary contributor to both mass and cost, smaller FMA designs are anticipated. The slumped glass mirror technology in development at NASA GSFC is appropriate for a wide variety of modular X-ray mirrors. As an example of scalability, the 1.8 m FMA design shown in Figure 6 has been developed. Note the same 12/24/24 module layout as the IXO FMA has been retained; the modules and structure have simply been scaled down. The percentage of mirror obscured by structure has been kept at 16% at 1.0 keV while the stiffness of the structure has increased due to the shorter beam spans and lighter modules. This suggests the potential for future decreases in FMA mass and/or increases in effective area with further design optimization.

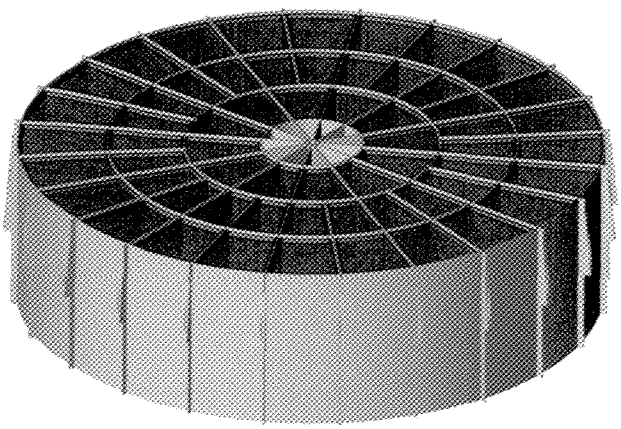

Parameter	Value
Structure Outer Diameter (m)	1.8
Focal Length (m)	10.0
Innermost Shell Diameter (mm)	299
Outermost Shell Diameter (mm)	1746
Number of Shells	227
Glass Mass (kg)	226
FMA Mass (kg)	512
1.0 keV Effective Area (m^2)	0.98
6.0 keV Effective Area (m^2)	0.23

Figure 6. Design and performance parameters for a 1.8 m X-ray mirror design.

3.2 Module Size Considerations

The layout and size of the modules is largely determined by the innermost and outermost segment diameters required to achieve the mission effective area requirements and the capability of the mirror technology to accommodate various azimuthal mirror spans [9]. As the mirror azimuthal span increases, the degree of constraint required to prevent gravity distortion during integration increases which may require technology changes.

Various layout options for a 1.8 m FMA are shown in Figure 7 with the corresponding mirror segment azimuthal spans shown in Table 8. The design assumes that symmetry is maintained such that each module is supported by a primary structural member and the radial size of the module rings is kept roughly equal [5]. It can be seen that as the size of the module decreases due to increased radial and azimuthal division, the range of mirror spans also decreases.

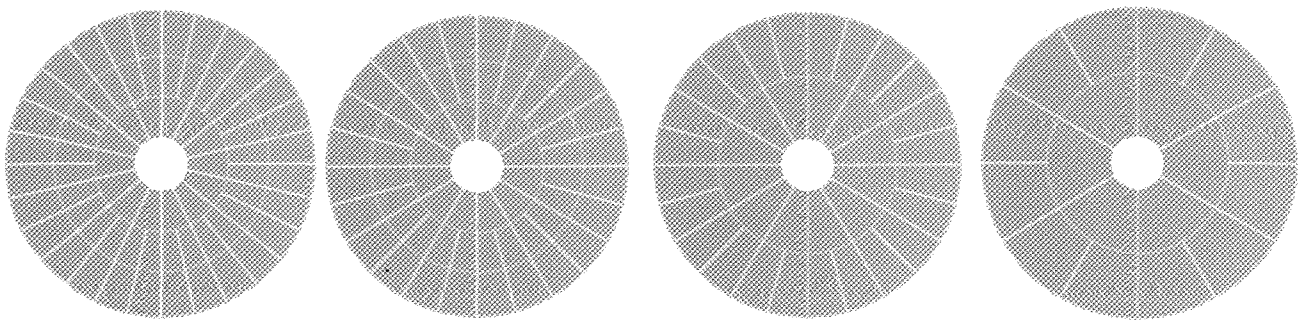

Figure 7. Module layout options, from left to right: 14/28/28, 12/24/24, 12/24, and 6/12.

Table 8. Mirror azimuthal span as a function of module layout for a 1.8 m X-ray mirror.

Layout	Number of Modules	Avg. Module Mass (kg)	Smallest Mirror Diameter (mm)	Largest Mirror Diameter (mm)	Range (mm)
14/28/28	70	5.2	52	181	129
12/24/24	60	6.0	48	214	166
1/2	36	10.0	48	253	205
1/2	18	20.0	142	520	378

Thus the range of azimuthal spans supported by the mirror technology drive the module size both in terms of the degree of azimuthal segmentation and the number of module rings. Consequently, both the number of modules and average module mass are also determined. Absent technology constraints on mirror span, the module size could be selected for other reasons such as minimizing the number of modules that need to be integrated, selecting a desired module mass, or minimizing cost. A FMA cost model including the module size as a factor is currently being developed. The module must also be sized to limit the mirror stress as discussed in section 2.3 and the gravity distortion as described in section 2.5 with smaller modules being superior in both cases.

4. CONCLUSIONS

Significant design and analysis work has been completed on the IXO mirror modules that can inform future module designs utilizing slump glass thin foil mirror technology. An extensive module material trade study has been performed including the development and testing of two custom materials matching the CTE of D263 glass. Kovar F15 has been selected as the baseline material due to its excellent CTE match and good machinability. A CLA has been performed for the IXO spacecraft leading to the development of high fidelity quasi-static loads applicable to future missions. Detailed stress analysis of the mirror segments coupled into the module structure has been performed and high sensitivity to module structure size demonstrated. The thermal control system design has been matured through successive iterations for STOP analysis demonstrating progress in reducing the effects of thermal distortion. Self weight distortion has been quantified for both integration and testing of modules. Future directions in module and FMA design have been explored including demonstration of the scalability of the IXO design and investigation of the effect of the module layout on mirror segment size, module size, and module performance.

REFERENCES

[1] J. Bookbinder, R. Smith, A. Hornschemeier, et al, "The Constellation-X Observatory" Proc. of SPIE Vol. 7011, 701102, 2008.

[2] Ph. Gondoin, D. de Chambure, K. van Katwijk, et al, "The XMM Telescope" Proc. of SPIE Vol. 2279, 1988.

[3] R. Petre, S. O'Dell ,"Thin shell segmented X-ray mirrors" X-Ray Optics and Instrumentation, Volume 2010, Article ID 412323.

[4] W. Zhang, K. Chan, G. Byron, et al, "Mirror technology development for the International X-ray Observatory mission" Proc. Of SPIE, 7437 (2009).

[5] R. McClelalnd, T. Carnahan, D. Robinson, T. Saha, "Design and Analysis of the International X-Ray Observatory Mirror Modules" Proc. Of SPIE Vol. 7732, 2010.

[6] M. K. Choi, "Thermal Optimization of IXO SXT FMA to Meet 20°C and Stringent Temperature Gradient Requirements and Heater Power Budget" Proc of AIAA Vol. 2010-6054, 2010.

[7] T. Saha, "Image defects from surface and alignment errors in grazing incidence telescopes" Opt. Eng. 29, 1296-1305 (1990).

[8] Y. Stockman, P. Barzin, H. Hansen, et al, "XMM flight mirror module testing" Proc. Of SPIE Vol. 3766, 1999.

[9] M. Biskach, R. McClelland, T. Saha, W. Zhang, "Size optimization for mirror segments for X-ray optics" Proc. of SPIE Vol. 8147, 2011.